Correlating Thermionic Emission with Specific Surface Reconstructions in a <100> Hydrogenated Single-Crystal Diamond

Hugo Dominguez-Andrade,* Julian Anaya, Alex Croot, Mattia Cattelan, Daniel J. Twitchen, Martin Kuball, and Neil A. Fox
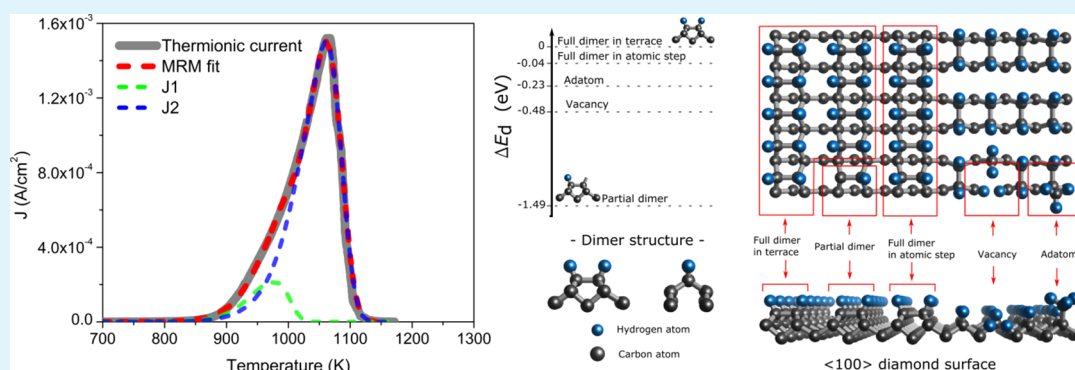
Read Online

ACCESS | Metrics & More | Article Recommendations | Supporting Information

ABSTRACT: Thermionic emission relies on the low work function and negative electron affinity of the, often functionalized, surface of the emitting material. However, there is little understanding of the interplay between thermionic emission and temperature-driven dynamic surface transformation processes as these are not represented on the traditional Richardson−Dushman equation for thermionic emission. Here, we show a new model for thermionic emission that can reproduce the effect of dynamic surface changes on the electron emission and correlate the components of the thermionic emission with specific surface reconstruction phases on the surface of the emitter. We use hydrogenated <100> single-crystal and polycrystalline diamonds as thermionic emitters to validate our model, which shows excellent agreement with the experimental data and could be applicable to other emitting materials. Furthermore, we find that tailoring the coverage of specific structures of the C(100)-(2 × 1):H surface reconstruction could increase the thermionic emission of diamond by several orders of magnitude.

KEYWORDS: thermionic, emission, diamond, hydrogen, surface

INTRODUCTION

Thermionic emission (TE) occurs when certain metals or semiconductors are heated beyond an emission threshold temperature, and thermally excited electrons have enough energy to overcome the surface potential barrier, leaving the solid with an associated kinetic energy.[1,2] TE has played a vital role in the technological development of electronic devices since the early 20th century owing to its use in vacuum valves for current rectification[3] employed in radars and analog computers. TE was later used in the development of X-ray sources,[4] pressure gauges, and thermionic energy converters for space applications.[5,6] The development of TE-based technologies was very intense up until the 1980s but then declined until the development of new materials with novel electronic properties prompted a revival of the research in this field. Among these materials were carbon nanotubes[7] and hydrogen-terminated diamond, which could emit thermionic electrons at significantly lower temperatures[8,9] than traditional thermionic materials (e.g., molybdenum with $T_{emission}$ >1700

K)[10] and therefore became candidates to be low-temperature electron emitters that would be more energetically efficient than traditional alternatives.

The capacity of a surface to produce TE relies strongly on the value of its work function (ϕ), which ideally should be kept as low as possible as it represents the surface potential barrier for electrons.[11] Low ϕ surfaces are usually achieved by chemisorbing specific species to create surface reconstructions with a strong surface dipole that lowers the surface potential barrier for electrons. To this end, monolayers of alkali metals[12,13] have been traditionally used to create such dipoles in refractory metals or semiconductors. In the case of diamond,

surface functionalization with alkalis[14,15] and other metals[16] has also been explored and showed the potential of the diamond surface to be modified with adsorbates. However, hydrogen termination, which generates a negative electron affinity surface,[17] has been the most widely studied owing to its simple fabrication process.[18−21] Yet, both alkali and hydrogen have a weak bond that causes thermal desorption from the substrate at high temperatures.[22] As a result, potential TE-based devices have to either make use of complex reservoir systems to continuously replenish the surface adatoms and/or operate at low temperatures at a low emission regime.

The Richardson−Dushman model, shown in eq 1, is commonly accepted as the theoretical basis of any model that describes the TE current from a surface,[23] but it was initially derived for ideal stable surfaces with a constant ϕ, disregarding any surface changes during the emission process. As a result, changes in the surface reconstruction phases of the emitter due to thermal desorption of the adsorbed species and its effects on TE are not reproduced by the Richardson−Dushman model or any current TE models. There is a significant body of work published in the field of barium cathodes in which the problem of barium depletion from impregnated barium cathodes is discussed[24−26] as well as its effects in emission with several models being proposed.[27,28] Nonetheless, although the causes for the decrease in the TE current at high temperatures have been studied previously,[29] there is little understanding of the interaction between the processes that are in play, i.e., TE, desorption kinetics of the adsorbates, and changes in the surface reconstruction.

$$J(T) = AT^2 e^{-\phi/kT} \tag{1}$$

Here, we present the first TE model that reproduces the electron emission behavior of a functionalized surface taking into account dynamic changes in the surface reconstruction phases and desorption kinetics of the adsorbate−substrate system. We show how the new TE model can be used to correlate the different TE components with specific surface reconstructions created by the adatoms and provide their energy of desorption. These are shown to possess marked differences in TE performance as well as having dissimilar bonding energies and surface coverages, which heavily influence the overall TE from the surface. We use both hydrogen-terminated <100> single-crystal and polycrystalline diamonds to validate our model and show how the different TE components are associated with surface structures, but the model could be applied to other materials. These results are supported by *ab initio* quantum mechanical simulations of several surface reconstructions and defects in diamond <100>. Finally, it is shown how, with selective surface modification, the TE emission from a diamond surface could be increased by several orders of magnitude, offering a new approach for the optimization and development of low-temperature TE-based devices.

EXPERIMENTAL DETAILS

Diamond Preparation. The diamond used for this study was a single-crystal diamond (type Ib) with a nitrogen impurity content of [N] ≈ 300 ppm produced by the high-pressure−high-temperature method and provided by Element6.Ltd. The diamond has a square shape (≈ 9.5 × 9.5 mm) and a thickness of ≈ 500 μm. One of the sides corresponding to the <100> orientation was provided polished. The hydrogen termination of the single-crystal diamond has been

carried out on a microwave chemical vapor deposition reactor under hydrogen plasma. The plasma conditions were P = 1500 W, pressure = 100 Torr, f_H = 300 sccm, $T_{substrate}$ = 470 °C, and t = 2 min.

Thermionic Emission Testing. Thermionic emission measurements were carried out on a high vacuum chamber with a base pressure of $P = 1 \times 10^{-6}$ mbar. The heating of the sample was done with a linearly polarized CO_2 laser (Synrad, Firestar V40 series) with a maximum power of 40 W that was fed inside the vacuum chamber through a viewport. The temperature of the sample was simultaneously monitored with a type-K thermocouple placed in tight contact with the sample and a two-color pyrometer (Spotmeter R160, Land instruments International. Ltd). The temperature measured by the pyrometer was the one used for the data presented in this study. The standard deviation of the two-color pyrometer is 2 K or $U_p = \pm 2.5 \cdot 10^{-3} \cdot T$, whichever is greater, and taking into account the whole temperature range of the experiments, it was always below 3 K. The thermionic current was measured by an ammeter (Keithley 2750, Tektronix). The standard deviation of the current measurements is $\pm 6.9 \times 10^{-7}$ A at most. The thermionic current from the diamond emitter was harvested with a molybdenum collector placed at a distance of 200 μm from the sample. To eliminate the space charge between the sample and collector and to saturate the thermionic emission current, a positive bias of 25 V was applied to the collector. A more detailed description of the thermionic testing setup, including temperature and current measurements, can be found elsewhere.[30]

Total hydrogen desorption experiments were performed by heating the diamond from 573 to 1193 K at a constant rate of 1 K/s followed by a cooling down to 573 K at the same rate following a triangular wave profile. The heating and cooling rate was controlled by a closed-loop feedback (PID control). Partial hydrogen desorption experiments were performed by heating the diamond from 573 to 1130 K at a rate of 1 K/s and then cooled again to 573 K at the same rate following a triangular wave profile. This process was repeated several times with not more than 15 s between cycles to avoid any hydrogen readsorption.

Work Function Measurements and Low Energy Electron Diffraction. The work function and low energy electron diffraction (LEED) measurements were conducted at the Bristol NanoESCA Facility (see Supporting Information SI.4).

Computational Methods. Periodic *ab initio* simulations were carried out using the generalized gradient approximation of Perdew, Burke, and Ernzerhof (PBE),[31] as implemented in the Cambridge serial total energy package (CASTEP) code[32] (see Supporting Information SI.5).

RESULTS AND DISCUSSION

A New Thermionic Emission Model. To understand the effect of the dynamic surface changes on the TE current and its relation with the different surface reconstructions, a new TE model was developed (see Supporting Information SI.1 for more details on the model). Upon functionalization of the surface of a monocrystalline material, certain adatoms will bond and modify the surface by changing the bond length of the surface atoms and causing a charge transfer between surface atoms and the adatoms. This process ultimately results in the formation of reconstructed phases on the surface with a defined structure and an associated surface dipole. These individual surface dipoles will cause the local ϕ to be modified, which in the case of some adsorbate−surface systems, would mean that the dipoles cause a reduction in the local ϕ when compared to that of the bare surface and the presence of a negative electron affinity. Therefore, given the appropriate temperature, these localized structures with low ϕ will act as electron emission centers as they present a less energy-expensive route for electrons to escape the surface. Moreover, the various surface phases will possess different properties

depending on the type of reconstruction, which include bond length, desorption energy (E_d), and ϕ. Thus, at elevated temperatures, each of these emission centers will thermionically emit electrons according to its ϕ with their thermal stability being dictated by its E_d, while the contribution to the total TE of a surface is given by the associated surface coverage (θ). Hence, the TE current from a functionalized surface taking into account surface changes due to thermal desorption effects from different surface phases can be described by

$$J(T, \theta, \phi) = \sum_i A_i T^2 e^{-\phi_i(\theta_i(T))/kT} \qquad (2)$$

where ϕ_i is a function of the coverage $\theta_i(T)$ for the surface reconstruction i to account for the initial linear work function decrease at low coverages upon surface functionalization and the subsequent work function increase due to depolarization effect of the dipole−dipole interaction[33] at medium-to-high coverages. Conversely, the evolution of the surface coverage with temperature can be described by

$$\theta_i(T) = \theta_{0-i} - \int_{T1}^{T2} \nu_i \theta_i^n e^{-E_{di}/kT} dT \qquad (3)$$

where θ_{0-i} is the initial coverage, n is the order of reaction, ν_i is the frequency factor, k is the Boltzmann constant, and E_{di} is the energy of desorption. Equation 2 along with Equation 3 will herein be called the modified Richardson−Dushman model (MRM) and in general is valid for any adsorbate−surface system with TE capabilities.

Thermionic Emission from the Single-Crystal Diamond. The validity of the MRM was tested with a hydrogen-terminated nitrogen-doped single-crystal diamond. A nitrogen-doped diamond was chosen for this tests as it is a well-known thermionic emitter that exhibits a n-type semiconducting behavior at moderate temperatures ($T > 300$ °C). TE is enabled in the nitrogen-doped diamond by the functionalization of its surface with hydrogen, which causes a significant decrease on its ϕ and the presence of a negative electron affinity. Moreover, the hydrogenated diamond surface is thermally unstable at elevated temperatures ($T > 600$ °C), which makes this surface an excellent material to study the effect of dynamic surfaces on TE. The TE from the <100> facet of a single-crystal diamond doped with nitrogen ([N] ≈ 300 ppm) and hydrogen termination is shown in Figure 1A. The TE plot corresponds to a thermal heating cycle starting at $T_{low} = 573$ K, rising up to $T_{high} = 1193$ K and then decreasing back to $T_{low} = 573$ K following a triangular pattern. The heating and cooling rates were 1 K/s. The plot shows that TE starts at $T_{start} \approx 723$ K and grows with an exponential trend until it peaks at $T_{Jmax} \approx 1060$ K producing a maximum current of $J_{max} \approx 1.53$ mA·cm^{-2}. This maximum is followed by a steep decrease of the current despite the fact that the temperature is still increasing. After the first heating cycle, no further TE current was detectable in subsequent heating cycles due to the loss of hydrogen termination. The traditional Richardson−Dushman model (eq 1) does not reproduce the observed TE behavior due to the dynamic character of the surface properties (see Figure S1 in Supporting Information SI.2). As we show in Figure 1A, the MRM successfully reproduces the experimental data for a single-crystal diamond with two convoluted components (J1 and J2), corresponding to two hydrogen surface reconstruction phases in the surface of the diamond with J2 accounting for most of the emission. The agreement between the experimental data and the modified Richardson
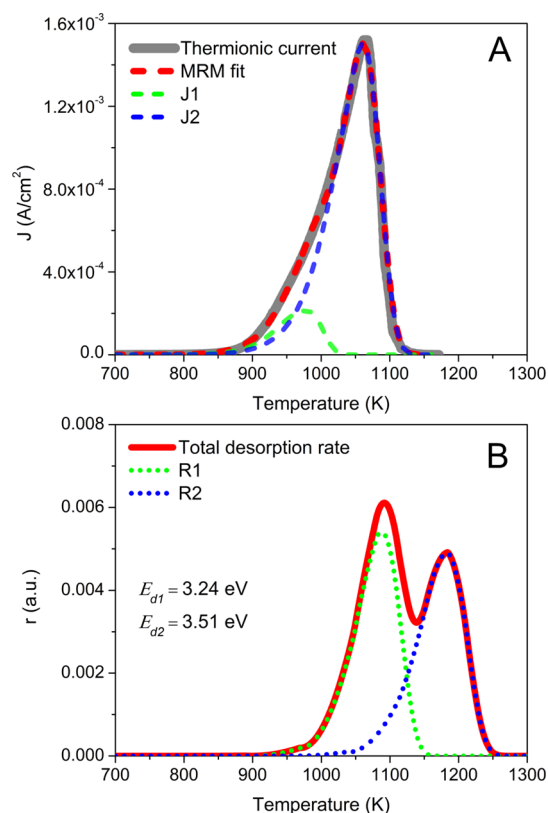

Figure 1. Thermionic emission from the hydrogen-terminated <100> single-crystal diamond fitted with the modified Richardson model. The hydrogenated single crystal was heated to from $T_{start} = 573$ K to $T_{max} = 1193$ K with a heating rate of $\beta = 1$ K/s and cooled (at a rate of $\beta = 1$ K/s) to $T_{start} = 573$ K following a triangular pattern. The measurements were performed under high vacuum with a base pressure of $P = 1 \times 10^{-6}$ mbar. (A) Thermionic emission current from the hydrogenated <100> single-crystal diamond shown in solid gray. The dashed red line shows the fit by the modified Richardson model, while the dashed green and blue lines represent the two components of the fit. The Richardson constant was calculated by the model to be $A_1 = A_2 = 79$ A·cm^{-2}·K^{-1}. The standard deviation for the thermionic current measurements is $\sigma_J < 6.21 \times 10^{-7}$ A and $\sigma_T < 3$ K for the temperature. (B) Desorption rate (r) plot for atomic hydrogen deconvoluted from the thermionic emission current by the application of the modified Richardson model. The solid red line represents the total desorption rate, whereas the dotted lines are the components of the total rate. These are correlated to the thermionic components, as indicated by the color coding and have an associated energy of desorption E_d. Their frequency factors were obtained from the MRM fitting and found to be $\nu_1 = 3.4 \times 10^{13}$ s^{-1} and $\nu_2 = 2.7 \times 10^{13}$ s^{-1} and the initial coverages $\theta_{0-1} = \theta_{0-2} \approx 0.43$.

model in the current decrease at $T > T_{Jmax}$ is especially relevant as, to the author's knowledge, it has never been previously reproduced by any other model.

The desorption kinetics parameters (E_{di}, ν_i, and θ_{0-i}) for atomic hydrogen on the <100> diamond surface as well as the Richardson constant were used as fitting parameters for the MRM and then used to elaborate the plot of Figure 1B. Figure 1B represents the desorption rate (r) of atomic hydrogen, and it shows two distinct components denoted as R1 and R2 with a respective initial coverage of $\theta_{0-1} = \theta_{0-2} \approx 0.43$. These components are respectively correlated with the thermionic current components (J1 and J2) shown in Figure 1A and have an associated desorption energy of $E_{d1} = 3.24$ eV and $E_{d2} = 3.51$ eV with an energy difference of $\Delta E_d = E_{d1} - E_{d2} = -0.29$
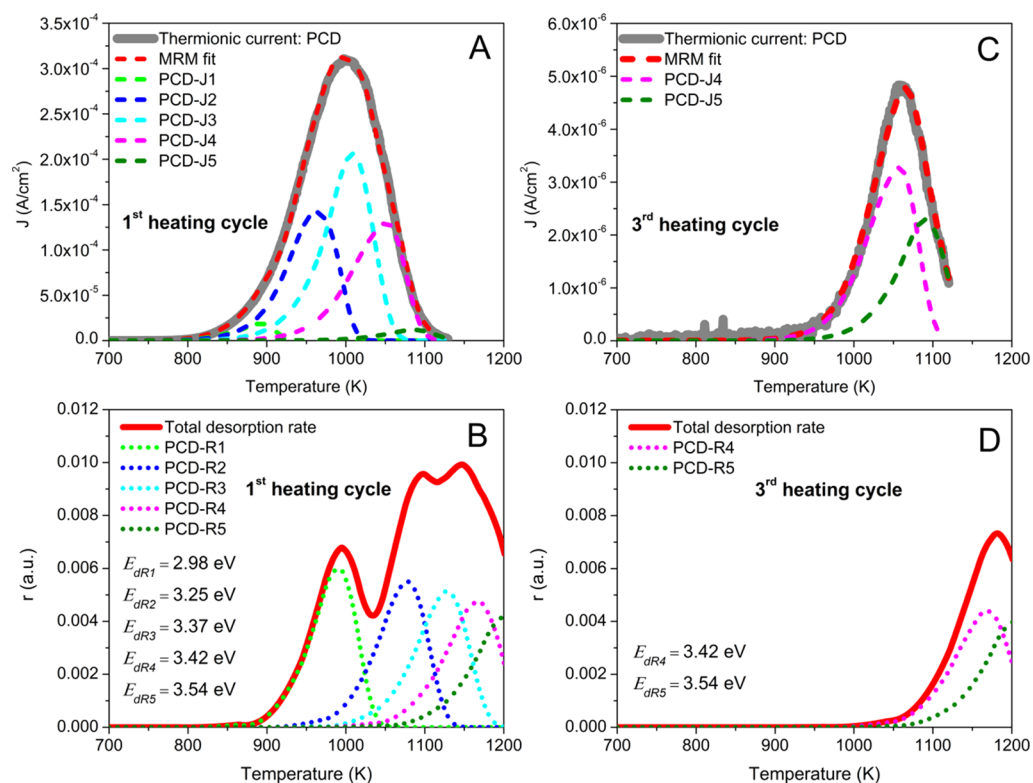
Figure 2. Thermionic emission from the hydrogen-terminated polycrystalline diamond fitted with the modified Richardson model. The hydrogenated diamond was heated to from T_{start} = 573 K to T_{max} = 1130 K with a heating rate of β = 1 K/s and cooled (at a rate of β = 1 K/s) to T_{start} = 573 K following a triangular pattern. This heating cycle process produced a partial desorption of the adsorbed hydrogen and was repeated several times without the rehydrogenation of the surface. The measurements were performed under high vacuum with a base pressure of P = 1 $\times$ 10^{-6} mbar. (A, C) Thermionic emission plots of the first and third heating cycles, respectively, shown in gray solid lines. The dashed red line represents the fitting of the modified Richardson model to the data. The other dashed lines represent the different components of the fit. The standard deviation for the thermionic current measurements is σ_J < 6.21 $\times$ 10^{-7} A and σ_T < 3 K for the temperature. (B, D) Desorption rate (r) plots for atomic hydrogen deconvoluted from the thermionic emission current by the application of the modified Richardson model. The solid red line represents the total desorption rate, whereas the dotted lines are the components of the total rate. These are correlated to the thermionic components, as indicated by the color coding and have an associated energy of desorption E_{dR}. The initial coverages for the components in the first cycle are θ_{0-1} = 0.207, θ_{0-2} = 0.206, θ_{0-3} = 0.203, θ_{0-4} = 0.197, and θ_{0-5} = 0.184, whereas those for the third cycle are θ_{0-4} = 0.183 and θ_{0-5} = 0.177.

---

eV. The values for the frequency factors are ν_1 = 3.4 $\times$ 10^{13} s^{-1} and ν_2 = 2.7 $\times$ 10^{13} s^{-1} and are in close agreement with the theoretical value of ν = 1 $\times$ 10^{13} s^{-1}. Additionally, the Richardson constants for J1 and J2 found by the MRM are A_1 = A_2 = 79 A·cm^{-2} K^{-1}, which are very close to the theoretical value of A = 120 A·cm^{-2} K^{-1}.

Desorption energies with values of 3.44[34] and 3.15 eV,[35] both with a ν = 1 $\times$ 10^{13} s^{-1}, have been reported previously for hydrogen on the <100> diamond surface, which are somewhat in the same range of our values. On the other hand, some authors reported lower values of the order of 1.60[36] and 1.69 eV[37] but both with a ν = 3 $\times$ 10^5 s^{-1} that deviates greatly from the theoretical value. Hence, we are inclined to believe that our results are more comparable with the first two values as their frequency factor is equal to the theoretical value and very close to ν_1 and ν_2.

The fact this manuscript reports two desorption energies as opposed to the literature that reports only one desorption energy for the <100> diamond surface might be caused by the fact that the experiment and MRM presented in this study are extremely sensitive to hydrogen desorption, so it allows for a straightforward deconvolution of the desorption parameters. The MRM was found to be fairly sensitive to the fitting parameters, especially to the desorption energies E_{di} and the

initial coverages θ_{0-i}, as a change of just 1% on their value would cause the value of the current J of the MRM to deviate more than 50% from the experimental data. Therefore, their values could be considered to have less than a 1% uncertainty (see Supporting Information SI.6).

Regarding the work function used in the MRM for the fit of experimental data, we used a coverage-dependent work function in the shape of a linear piecewise function (ϕ = ϕ(θ)). In our case, we assumed that the work function of all emitting areas of the surface would follow the same piecewise function, despite having different kinetic desorption parameters as to simplify the application of the MRM to the experimental data. This function can be defined with just three pairs of coordinates (θ, ϕ) for θ = 0, 0.5, and 1. The work function values used for the function were ϕ_0 = 7 eV, $\phi_{0.5}$ = 1.5 eV, and ϕ_1 = 2 eV. These are discussed in more detail in Supporting Information SI.7. While $\phi_{0.5}$ and ϕ_1 were chosen based in experimental and literature values, the value of ϕ_0 had to be increased with respect to the value reported in the literature (4.7 eV)[38] in order for the MRM to fit the experimental data at low coverages. The increased apparent value of the work function at low coverages is most probably caused by the effect on the work function of having a "patchy surface" at low coverages,[39] while a decrease on the surface
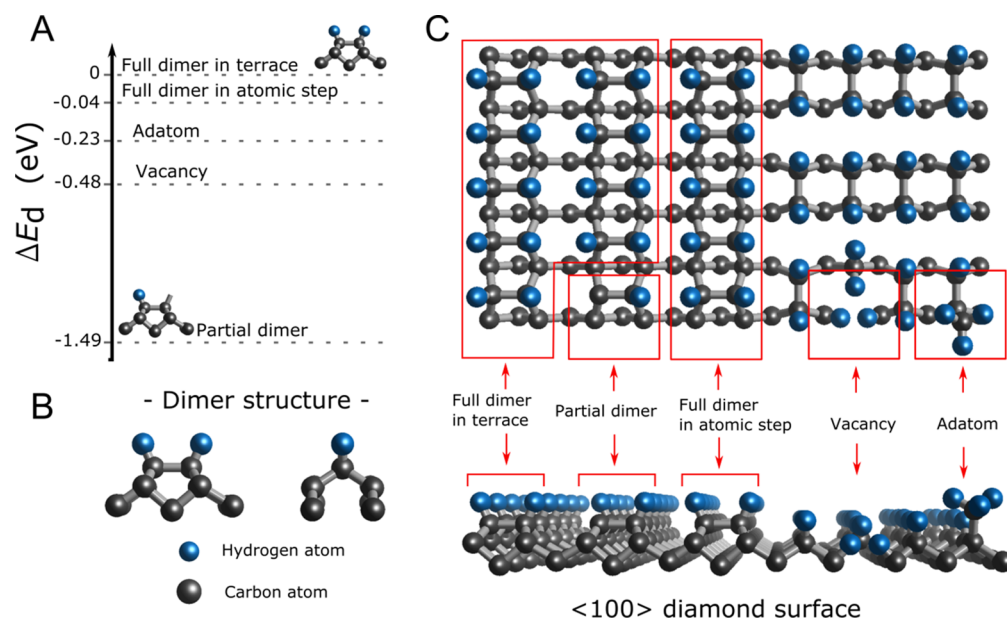
Figure 3. *Ab initio* simulation of desorption energies for atomic hydrogen in <100> single-crystal diamond. (A) Energy of desorption difference ($\Delta E_d = E_{di} - E_{d2}$) of atomic hydrogen desorbing from different sites normalized to the desorption energy of a full dimer E_{d2}. (B) Structure of a fully terminated carbon dimer on the <100> surface. (C) Diagram of the different surface bonding structures of hydrogen in the <100> diamond surface that were simulated in this study. Dark spheres represent carbon atoms, while dark blue spheres represent hydrogen atoms. The atomic representations in this figure were generated with the 3D visualization program VESTA.[59]

conductivity due to hydrogen desorption[21] and the temperature dependence of the work function[40] might contribute to this behavior to a certain extent. Overall, the matter with ϕ_0 means that the MRM is somewhat limited at low coverages as it does not take into account the effects mentioned above in its present form. Nonetheless, the MRM still provides a very significant improvement when analyzing thermionic emission data when compared to just using the Richardson equation.

Thermionic Emission from the Polycrystalline Diamond. The existence of the different diamond surface phases observed when applying the MRM was further tested by applying the model to the TE produced by hydrogenated nitrogen-doped polycrystalline diamond as it has a more complex surface. In this case, the heating cycle was performed similarly to the single crystal with the exception that the maximum temperature was slightly lower (T_{high} = 1130 K). The consequence of this change was that several heating cycles were necessary to desorb all the hydrogen present in the surface. The results of this experiment are shown in Figure 2 where the TE fitted with the MRM and the deconvoluted desorption plots for the first (Figure 2A,C) and third (Figure 2B,D) heating cycles are plotted. The MRM was successfully applied to the polycrystalline diamond and could reproduce the experimental data, but it still required a minimum of five components on the first heating cycle due to the elevated number of surface phases on its surface. Subsequent heating cycles continue to desorb the remaining hydrogen of the surface, causing the surface phases with a lower desorption energy to reduce their coverage or disappear. This can be clearly observed in Figure 2C,D where we can see that the current and desorption rate components PCD-J1 (PCD-R1), PCD-J2 (PCD-R2), and PCD-J3 (PCD-R3) have completely disappeared. On the other hand, the components PCD-J4 (PCD-R4) and PCD-J5 (PCD-R5) are still present but their surface coverage has decreased as well as the thermionic current produced by them. Remarkably, these components

maintain the same E_{di} in all the heating cycles where the MRM is applied independently and only the surface coverage is seen to decrease. This shows that the modified Richardson model can produce consistent results even in complex surfaces.

***Ab Initio* Simulation of the Hydrogenated <100> Diamond Surface.** An ideal hydrogen-terminated <100> single-crystal diamond presents a C(100)-(2 × 1):H surface reconstruction where carbon atoms form dimer rows across the atomically flat terraces and are terminated by hydrogen atoms with single bonds [HC−CH].[41] There are some reports about the existence of a C(100)-(1 × 1):H reconstruction;[42] however, its existence is still uncertain[43] and the consensus in the literature is currently the C(100)-(2 × 1):H reconstruction.[38,44−48] Hence, the *ab initio* simulations of this study are focused on the latter. This reconstruction was found to be present on the hydrogenated <100> single-crystal diamond used for this study according to low energy electron diffraction experiments (see Figure S2 in Supporting Information SI.3). However, real surfaces have multiple defects, i.e., atomic step edges, vacancies, and adatoms, and these might cause the formation of alternative hydrogen surface reconstructions deviating from the ideal case of a perfect defect-free surface. Hence, to correlate the components J1 (R1) and J2 (R2) of the TE current in the hydrogenated <100> single-crystal diamond with the present surface phases, quantum mechanical *ab initio* simulations of the reconstructed surface and several surface defects were performed.

The desorption energy of the ideal C(100)-(2 × 1):H surface reconstruction and other surface structures and defects obtained with *ab initio* simulations are shown in Figure 3 normalized to the desorption energy of the full dimer E_{d2}. These show that the most stable surface reconstruction is the C(100)-(2 × 1):H, corresponding to a fully hydrogenated dimer [HC−CH] on a flat terrace as it has the highest desorption energy ($E_{d\text{-full\_terrace}}$) among the studied structures. As a result, we believe that the component J2 of the TE
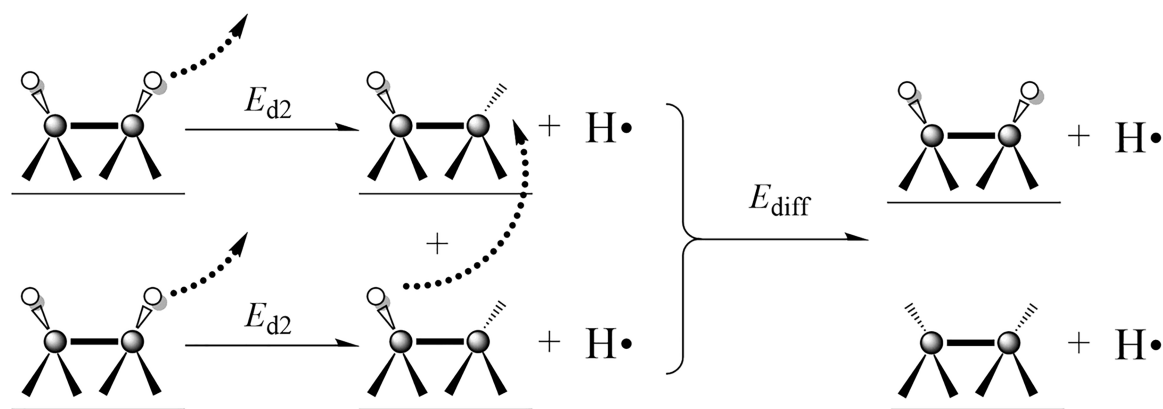
Figure 4. Proposed desorption path for hydrogen on the <100> surface of single-crystal diamond. Hydrogen desorbs from the fully terminated dimer with a desorption energy of $E_{d2} = 3.51$ eV, generating a partially terminated dimer and a hydrogen radical. Then, another hydrogen from a partially terminated dimer diffuses (E_{diff}) across the surface to form a fully terminated and an unterminated dimer. Dark circles represent carbon atoms, while white circles represent hydrogen atoms.

current, which experimentally shows the highest desorption energy, originates in the fully hydrogenated dimers [HC−CH] on a flat terrace.

The literature regarding the simulation of hydrogen desorption for the <100> single-crystal diamond is mostly concerned in simulating the desorption energies of the first and second hydrogen from the monohydrogenated dimer on a sequential fashion. This is an E_{d1H} for [HC−CH] → [HC−C*] + H$_{(g)}$, and an E_{d2H} for [HC−C*] → [*C−C*] +2H$_{(g)}$. When examining $\Delta E_{d1-2} = E_{d1H} - E_{d2H}$, the reported values are −1.45,[49] −1,[50] −0.7,[51] −0.6,[52] and −0.27 eV.[53] While our simulation shows a value of −1.49 eV in agreement with the work of Brenner,[49] the literature values span over a wide range with no clear consensus.

Considering the energy diagram in Figure 3, the ΔE_d between $E_{d\text{-full\_terrace}}$ and other surface defects as well as fully terminated dimers near atomic step edges is $\Delta E_d > -0.48$ eV with the only exception of the partially terminated dimer [HC−C*], which has an $\Delta E_d \approx -1.49$ eV. Taking into account that, for the component J1, the experimental value of the desorption energy difference is $\Delta E_d = E_{d1} - E_{d2} = -0.29$ eV, it is in principle not possible to identify a specific surface structure as the cause for the component J1 by looking at the surface simulations. Nevertheless, considering that the initial coverage of the reconstruction responsible for the component J1 is $\theta_{0-1} \approx 0.43$, the only surface structure that can reasonably have such a high initial coverage, apart from the fully terminated dimer on a flat terrace, is the fully terminated dimer reconstruction [HC−CH] adjacent to an atomic step edge. This high coverage of step edges in the diamond surface has been shown by scanning tunneling microscopy studies of diamond surfaces by several groups.[54−56] Fully terminated dimers placed adjacent to an atomic step edge will have a slight structural distortion when compared with dimers further away from the step edge, causing a small difference in desorption energy ΔE_d between the two cases. As a result, we could tentatively assign the origin of the component J1 of the TE current to the fully terminated dimers adjacent to atomic step edges.

During the TE process at elevated temperatures, atomic hydrogen is thermally desorbed from fully terminated dimers, thus creating partially terminated dimers [HC−C*] that would subsequently desorb. However, the high temperatures on the diamond enable hydrogen diffusion across the surface. So, a hydrogen atom from a partially terminated dimer has enough thermal energy to hop between dimers until it finds another partially terminated dimer to form a full dimer, which is more energetically favorable than having two partially terminated dimers (see Figure 4). This is possible due to the fact that diffusion energy for hydrogen in the diamond surface is $E_{diff} \approx$ 0.5−1.5 eV,[57,58] which is lower than the E_{di} for both components J1 and J2 and that for a partial dimer $E_{d\text{-partial}} \approx$ 2 eV.

Predicted Thermionic Emission Current from Hydrogenated Single-Crystal Diamond for Different Coverages. The parameters (E_{di}, ν_i, θ_{0-i}, and A_i) of the surface dipoles of the hydrogen-terminated single-crystal diamond were extracted, applying the MRM to the experimental TE data. As a result, it was possible to exploit the MRM to investigate the electron emission behavior of the said surface under different hydrogen surface coverage conditions. Figure 5 shows plots of the TE for the hydrogen-terminated single-crystal diamond for different coverages of fully terminated dimers on a flat terrace. These plots mimic the experimental heating profiles used in the experiments shown in Figures 1 and 2.

As the work function $\phi = \phi(\theta)$ is a function of the coverage (see Supporting information SI.7), the effect of an increase of the coverage from $\theta = 0$ to 0.5 will be two-fold. First, the emission surface per unit area will obviously increase, and second and more importantly, the work function will decrease until it reaches a minimum at $\theta = 0.5$. Mathematically, this means that the exponential term in eq 2 approaches 1 at lower temperatures so that the quadratic temperature dependence of the TE current starts earlier. In Figure 5, it is shown how this increase in the coverage has a double effect. First, it lowers the temperature at which TE starts from $T_{start} \approx 900$ K down to $T_{start} \approx 400$ K. Second, it increases considerably the TE current. Both effects are beneficial because they would reduce the working temperature and increase the power output of a potential device based on this type of surface. Yet, these beneficial effects occur up to a value of $\theta \approx 0.55$. After that, a reversal of these effects is observed with the T_{start} increasing again to 550 K and the TE current decreasing at least a couple of orders of magnitude. This is the consequence of the hydrogen dipole depolarization on the dimers due to the dipole−dipole interaction mentioned previously, which is included in the MRM. Such a depolarization causes an
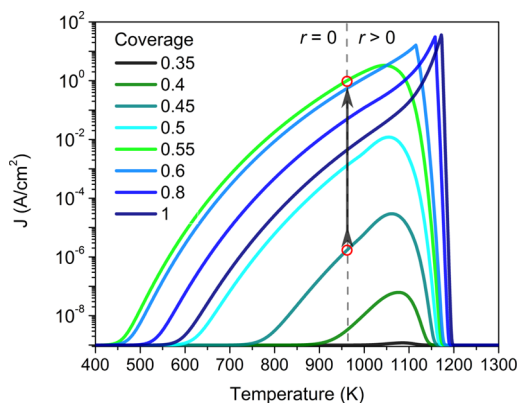
Figure 5. Predicted thermionic current from a hydrogenated <100> single crystal-diamond surface for different surface coverages. These estimations were obtained with the modified Richardson model by extrapolating the thermionic current for various degrees of initial coverages of the fully terminated dimer, and using the desorption energy, the Richardson constant and frequency factor that were obtained by fitting the MRM to the experimental data. For the sake of simplicity, the coverage of any other surface phases was kept as zero, which means that the predicted thermionic current originates only from fully terminated dimers. This corresponds to component P2 in Figure 2 with an E_d = 3.51 eV. The gray dashed vertical line at T = 960 K indicates a temperature below which the desorption rate can be considered negligible ($r \approx 0$) so that the hydrogen would be thermally stable. At this temperature, the current increases with the initial coverage of fully terminated dimers up to $\theta_0 \approx 0.55$ where it reaches a maximum before decreasing again due to a depolarization of the hydrogen dipoles also known as the topping effect.

increase of the work function of the surface at high coverages that effectively increases the surface potential barrier for electrons and lowers the TE.

Our model predicted that, if the surface coverage for the fully terminated dimer on a flat terrace were to be increased from θ = 0.43 (value found in the experimental results) to 0.55 and the operation temperature kept below $T \approx 960$ K so that the hydrogen desorption rate is $r \approx 0$, then it could be possible to permanently sustain a TE emission current of $J \approx 1$ A·cm^{-2}. This is an increase in the current of 7 orders of magnitude compared to the experimental results presented in this study and highlights the potential for this type of adsorbate−surface system to be used as an electron emitter.

CONCLUSIONS

A new material-independent model for thermionic emission based on the Richardson−Dushman equation has been presented and successfully applied to the TE from a hydrogen-terminated single-crystal diamond. Our proposed MRM successfully reproduced, for the first time, the TE behavior of functionalized surfaces in diamond, accounting for the effect of dynamic changes in surface phases due to thermal desorption of the adsorbates. It was shown that it is possible to extract the values for energy of desorption (E_d) and initial coverage (θ_0) of the hydrogen adsorbed in the diamond surface with just TE data without using the traditional techniques for these type of measurements. More importantly, in the case of the hydrogenated <100> single-crystal diamond, we identified the fully terminated dimers of the C(100)-(2 × 1):H surface reconstruction on flat terraces as the origin of the majority of the TE, which is also the most thermally stable form of hydrogen on the diamond <100> surface. We show

that, according to predictions from our model, a sustained current of $J \approx 1$ A·cm^{-2} could be achieved if the surface coverage of fully terminated dimers in flat terraces was to be increased from θ = 0.43 to 0.55 and the surface temperature kept below $T \approx 960$ K to avoid hydrogen thermal desorption. Thus, the results presented here provide new insight into the operation of TE on dynamic surfaces and opens a new avenue for the study and optimization of thermionic emitting surfaces for electron generation or energy harvesting applications. Additionally, we believe that our research could also be relevant for the understanding of the behavior of rectifying junctions as our model could be used to factor in inhomogeneities or degradation in the junction when analyzing its current characteristics.

ASSOCIATED CONTENT

ⓈⒾ Supporting Information

The Supporting Information is available free of charge at https://pubs.acs.org/doi/10.1021/acsami.0c01677.

> Modified Richardson−Dushman model (MRM) (SI.1), Richardson−Dushman equation fit to experimental thermionic emission data (SI.2), work function measurement of the hydrogen-terminated <100> single-crystal diamond and LEED pattern of the same surface (SI.3), and experimental details of the work function and LEED measurements (SI.4), computational methods - *ab initio* simulations (SI.5), parameter sensitivity on the MRM (SI.6), work function piece-wise function (SI.7) (PDF)

AUTHOR INFORMATION

Corresponding Author

Hugo Dominguez-Andrade − *School of Physics, H. H. Wills Physics Laboratory, University of Bristol, Bristol BS8 1TL, U.K.;* ⓘ orcid.org/0000-0002-9208-2001;
Email: hugo.dominguez@bristol.ac.uk

Authors

Julian Anaya − *School of Physics, H. H. Wills Physics Laboratory, University of Bristol, Bristol BS8 1TL, U.K.*
Alex Croot − *School of Physics, H. H. Wills Physics Laboratory, University of Bristol, Bristol BS8 1TL, U.K.*
Mattia Cattelan − *School of Chemistry, University of Bristol, Bristol BS8 1TS, U.K.;* ⓘ orcid.org/0000-0001-9314-1475
Daniel J. Twitchen − *Element Six Ltd, Ascot SL5 8BP, U.K.*
Martin Kuball − *Center for Device Thermography, H. H. Wills Physics Laboratory, University of Bristol, Bristol BS8 1TL, U.K.*
Neil A. Fox − *School of Physics, H. H. Wills Physics Laboratory and School of Chemistry, University of Bristol, Bristol BS8 1TL, U.K.*

Complete contact information is available at:
https://pubs.acs.org/10.1021/acsami.0c01677

Author Contributions

The manuscript was written through contributions of all authors. All authors have given approval to the final version of the manuscript.

Notes

The authors declare no competing financial interest.

ACKNOWLEDGMENTS

ABBREVIATIONS

TE, thermionic emission
MRM, modified Richardson−Dushman model

REFERENCES

(1) Preece, W. H. II. On a Peculiar Behaviour of Glow-Lamps When Raised to High Incandescence. *Proc. R. Soc. London* **1884**, *38*, 219−230.

(2) Elster, J.; Geitel, H. Ueber Die Electricitätserregung Beim Contact Verdünnter Gase Mit Galvanisch Glühenden Drähten. *Ann. Phys. Chem.* **1889**, *273*, 315−329.

(3) Fleming, J. A. Improvements in Instruments for Detecting and Measuring Alternating Electric Currents. GBD190424850 19041116, 1904.

(4) Coolidge, W. D. A Powerful Röntgen Ray Tube with a Pure Electron Discharge. *Phys. Rev.* **1913**, *2*, 409−430.

(5) Gryaznov, G. M.; Zhabotinskii, E. E.; Zrodnikov, A. V.; Nikolaev, Y. V.; Ponomarev-Stepnoi, N. N.; Pupko, V. Y.; Serbin, V. I.; Usov, V. A. Thermoemission Reactor-Converters for Nuclear Power Units in Outer Space. *Sov. At. Energy* **1989**, *66*, 414−418.

(6) Hatsopoulos, G. N.; Gyftopoulos, E. P. *Thermionic Energy Conversion. Volume I. Processes and Devices*; The MIT Press: 1973.

(7) Schwede, J. W.; Bargatin, I.; Riley, D. C.; Hardin, B. E.; Rosenthal, S. J.; Sun, Y.; Schmitt, F.; Pianetta, P.; Howe, R. T.; Shen, Z.-X.; Melosh, N. A. Photon-Enhanced Thermionic Emission for Solar Concentrator Systems. *Nat. Mater.* **2010**, *9*, 762−767.

(8) Hatta, A.; Ogawa, K.; Eimori, N.; Deguchi, M.; Kitabatake, M.; Ito, T.; Hiraki, A. Electron Emitter Device of NEA Diamond Thin Film. *Appl. Surf. Sci.* **1997**, *117-118*, 592−596.

(9) Koeck, F. A. M.; Garguilo, J. M.; Nemanich, R. J. On the Thermionic Emission from Nitrogen-Doped Diamond Films with Respect to Energy Conversion. *Diamond Relat. Mater.* **2004**, *13*, 2052−2055.

(10) Gubbels, G. H. M.; Wolff, L. R.; Metselaar, R. A Thermionic Energy Converter with Polycrystalline Molybdenum Electrodes. *J. Appl. Phys.* **1988**, *64*, 1508−1512.

(11) Hölzl, J.; Schulte, F. K.; Wagner, H. *Solid Surface Physics Springer Tracts in Modern Physics*; Hölzl, J., Schulte, F. K., Wagner, H., Eds. Springer-Verlag: Berlin/Heidelberg, 1979; Vol. 85, DOI: 10.1007/BFb0048918.

(12) Yakovkin, I. N.; Katrich, G. A.; Loburets, A. T.; Vedula, Y. S.; Naumovets, A. G. Alkaline-Earth Overlayers on Furrowed Transition Metal Surfaces: An Example of Tailoring the Surface Properties. *Prog. Surf. Sci.* **1998**, *59*, 355−365.

(13) Medvedev, V. K.; Naumovets, A. G.; Smereka, T. P. Lithium Adsorption on the (112) Face of Tungsten. *Surf. Sci.* **1973**, *34*, 368−384.

(14) Martin, T. L.; O'Donnell, K. M.; Shiozawa, H.; Giusca, C. E.; Fox, N. A.; Silva, S. R. P.; Cherns, D. Lithium Monolayers on Single Crystal C(100) Oxygen-Terminated Diamond. *MRS Online Proc.* **2011**, *1282*.

(15) O'Donnell, K. M.; Edmonds, M. T.; Ristein, J.; Tadich, A.; Thomsen, L.; Wu, Q.-H.; Pakes, C. I.; Ley, L. Diamond Surfaces with Air-Stable Negative Electron Affinity and Giant Electron Yield Enhancement. *Adv. Funct. Mater.* **2013**, *23*, 5608−5614.

(16) O'Donnell, K. M.; Edmonds, M. T.; Tadich, A.; Thomsen, L.; Stacey, A.; Schenk, A.; Pakes, C. I.; Ley, L. Extremely High Negative Electron Affinity of Diamond via Magnesium Adsorption. *Phys. Rev. B* **2015**, *92*, No. 035303.

(17) Takeuchi, D.; Ri, S.-G.; Kato, H.; Nebel, C. E.; Yamasaki, S. Negative Electron Affinity on Hydrogen Terminated Diamond. *Phys. Status Solidi A* **2005**, *202*, 2098−2103.

(18) Ristein, J. Surface Science of Diamond: Familiar and Amazing. *Surf. Sci.* **2006**, *600*, 3677−3689.

(19) Maier, F.; Graupner, R.; Hollering, M.; Hammer, L.; Ristein, J.; Ley, L. The Hydrogenated and Bare Diamond (110) Surface: A Combined LEED-, XPS-, and ARPES Study. *Surf. Sci.* **1999**, *443*, 177−185.

(20) Koeck, F. A. M.; Nemanich, R. J. Emission Characterization from Nitrogen-Doped Diamond with Respect to Energy Conversion. *Diamond Relat. Mater.* **2006**, *15*, 217−220.

(21) Williams, O. A.; Jackman, R. B. Surface Conductivity on Hydrogen Terminated Diamond. *Semicond. Sci. Technol.* **2003**, *18*, S34−S40.

(22) Schulberg, M. T.; Fox, C. A.; Kubiak, G. D.; Stulen, R. H. Hydrogen Desorption from Chemical Vapor Deposited Diamond Films. *J. Appl. PhysJournal of Applied Physics* **1995**, *77*, 3484.

(23) Richardson, O. W. Thermionic Phenomena and the Laws Which Govern Them. *Nobel Lecture.* **1929**.

(24) Coletti, M.; Gabriel, S. B. A Model for Barium Oxide Depletion From Hollow Cathode Inserts. *IEEE Trans. Plasma Sci.* **2009**, *37*, 58−66.

(25) Roquais, J. M.; Poret, F.; le Doze, R.; Ricaud, J. L.; Monterrin, A.; Steinbrunn, A. Barium Depletion Study on Impregnated Cathodes and Lifetime Prediction. *Appl. Surf. Sci.* **2003**, *215*, 5−17.

(26) Forman, R. Surface Studies of Barium and Barium Oxide on Tungsten and Its Application to Understanding the Mechanism of Operation of an Impregnated Tungsten Cathode. *J. Appl. Phys.* **1976**, *47*, 5272−5279.

(27) Longo, R. T. Physics of Thermionic Dispenser Cathode Aging. *J. Appl. Phys.* **2003**, *94*, 6966−6975.

(28) Mita, N. Degradation Factors of a Coated Impregnated Cathode. *IEEE Trans. Electron Devices* **1992**, *39*, 2172−2175.

(29) Paxton, W. F.; Steigerwald, A.; Howell, M.; Tolk, N.; Kang, W. P.; Davidson, J. L. The Effect of Hydrogen Desorption Kinetics on Thermionic Emission from Polycrystalline Chemical Vapor Deposited Diamond. *Appl. Phys. Lett.* **2012**, *101*, 243509.

(30) Dominguez-Andrade, H.; Croot, A.; Wan, G.; Smith, J. A.; Fox, N. A. Characterisation of Thermionic Emission Current with a Laser-Heated System. *Rev. Sci. Instrum.* **2019**, *90*, No. 045110.

(31) Perdew, J. P.; Burke, K.; Ernzerhof, M. Generalized Gradient Approximation Made Simple. *Phys. Rev. Lett.* **1996**, *77*, 3865−3868.

(32) Clark, S. J.; Segall, M. D.; Pickard, C. J.; Hasnip, P. J.; Probert, M. I. J.; Refson, K.; Payne, M. C. First Principles Methods Using CASTEP. *Z. Kristallogr. − Cryst. Mater.* **2005**, *220*, 567−570.

(33) Topping, J. On the Mutual Potential Energy of a Plane Network of Doublets. *Proc. R. Soc. A: Mat., Phys. Eng. Sci.* **1927**, *114*, 67−72.

(34) Yang, Y. L.; Struck, L. M.; Sutcu, L. F.; D'Evelyn, M. P. Chemistry of Hydrogen on Diamond (100). *Thin Solid Films* **1993**, *225*, 203−211.

(35) Thomas, R. E.; Rudder, R. A.; Markunas, R. J. Thermal Desorption from Hydrogenated and Oxygenated Diamond (100) Surfaces. *J. Vac. Sci. Technol., A* **1992**, *10*, 2451−2457.

(36) Hamza, A. V.; Kubiak, G. D.; Stulen, R. H. Hydrogen Chemisorption and the Structure of the Diamond C(100)-(2 × 1) Surface. *Surf. Sci.* **1990**, *237*, 35−52.

(37) McGonigal, M.; Kempel, M. L.; Hammond, M. S.; Jamison, K. D. Isothermal Hydrogen Desorption from the Diamond (100)2×1 Surface. *J. Vac. Sci. Technol., A* **1996**, *14*, 2308−2314.

(38) Diederich, L.; Küttel, O.; Ruffieux, P.; Pillo, T.; Aebi, P.; Schlapbach, L. Photoelectron Emission from Nitrogen- and Boron-Doped Diamond (100) Surfaces. *Surf. Sci.* **1998**, *417*, 41−52.

(39) Herring, C.; Nichols, M. H. Thermionic Emission. *Rev. Mod. Phys..* **1949**, *21*, 185.

(40) Mönch, W.; Enninghorst, R.; Clemens, H. J. An Experimental Study on the Temperature Dependence of Electron Affinity and Ionization Energy at Semiconductor Surfaces. *Surface Science Letters* **1981**, *102*, L54−L58.

(41) Kawarada, H.; Sasaki, H.; Sato, A. Scanning-Tunneling-Microscope Observation of the Homoepitaxial Diamond (001) 2×1 Reconstruction Observed under Atmospheric Pressure. *Phys. Rev. B* **1995**, *52*, 11351−11358.

(42) Kawarada, H. Hydrogen-Terminated Diamond Surfaces and Interfaces. *Surf. Sci. Rep.* **1996**, *26*, 205−206.

(43) Graupner, R.; Maier, F.; Ristein, J.; Ley, L.; Jung, C. High-Resolution Surface-Sensitive C 1s Core-Level Spectra of Clean and Hydrogen-Terminated Diamond (100) and (111) Surfaces. *Phys. Rev. B* **1998**, *57*, 12397−12409.

(44) Baumann, P. K.; Nemanich, R. J. Surface Cleaning, Electronic States and Electron Affinity of Diamond (100), (111) and (110) Surfaces. *Surf. Sci.* **1998**, *409*, 320−335.

(45) Nützenadel, C.; Küttel, O. M.; Diederich, L.; Maillard-Schaller, E.; Gröning, O.; Schlapbach, L. STM Investigations with Atomic Resolution on the (2 × 1) Monohydride Natural Doped Diamond (100) Surface. *Surf. Sci.* **1996**, *369*, L111−L116.

(46) Hellner, L.; Mayne, A. J.; Bernard, R.; Dujardin, G. Hydrogenated Diamond Crystal C(100) Conductivity Studied by STM. *Diamond Relat. Mater.* **2005**, *14*, 1529−1534.

(47) Bobrov, K.; Mayne, A.; Comtet, G.; Dujardin, G.; Hellner, L.; Hoffman, A. Atomic-Scale Visualization and Surface Electronic Structure of the Hydrogenated Diamond C(100)-(2x1):H Surface. *Phys. Rev. B* **2003**, *68*, 195416.

(48) Diederich, L.; Küttel, O. M.; Aebi, P.; Schlapbach, L. Electron Emission and NEA from Differently Terminated, Doped and Oriented Diamond Surfaces. *Diamond Relat. Mater.* **1999**, *8*, 743−747.

(49) Brenner, D. W. Empirical Potential for Hydrocarbons for Use in Simulating the Chemical Vapor Deposition of Diamond Films. *Phys. Rev. B* **1990**, *42*, 9458−9471.

(50) Dawnkaski, E. J.; Srivastava, D.; Garrison, B. J. Time Dependent Monte Carlo Simulations of H Reactions on the Diamond {001}(2×1) Surface under Chemical Vapor Deposition Conditions. *The Journal of Chemical Physics* **1995**, *102*, 9401−9411.

(51) Zilibotti, G.; Corni, S.; Righi, M. C. Formation Energy of Dangling Bonds on Hydrogenated Diamond Surfaces: A First-Principles Study. *Phys. Rev. B* **2012**, *85*, No. 033406.

(52) Hukka, T. I.; Pakkanen, T. A.; D'Evelyn, M. P. Chemisorption of Hydrogen on the Diamond (100)2 .Times. 1 Surface: An Ab Initio Study. *J. Phys. Chem.* **1994**, *98*, 12420−12430.

(53) Jing, Z.; Whitten, J. L. Ab Initio Studies of H Chemisorption on C(100) Surface. *Surf. Sci.* **1994**, *314*, 300−306.

(54) Stallcup, R. E.; Perez, J. M. Scanning Tunneling Microscopy Studies of Temperature-Dependent Etching of Diamond (100) by Atomic Hydrogen. *Phys. Rev. Lett.* **2001**, *86*, 3368−3371.

(55) Bobrov, K.; Mayne, A. J.; Hoffman, A.; Dujardin, G. Atomic-Scale Desorption of Hydrogen from Hydrogenated Diamond Surfaces Using the STM. *Surf. Sci.* **2003**, *528*, 138−143.

(56) Bobrov, K.; Mayne, A. J.; Dujardin, G. Atomic-Scale Imaging of Insulating Diamond through Resonant Electron Injection. *Nature* **2001**, *413*, 616−619.

(57) Kanai, C.; Shichibu, Y.; Watanabe, K.; Takakuwa, Y. Ab Initio Study on Surface Segregation of Hydrogen from Diamond C(100) Surfaces. *Phys. Rev. B* **2002**, *65*, 153312.

(58) Okamoto, Y. Hybrid Density-Functional Calculations of the Reactions of a H_2 Molecule on C, Si, and Ge(001) Surfaces. *J. Phys. Chem. B* **2002**, *106*, 570−573.

(59) Momma, K.; Izumi, F. VESTA 3 for Three-Dimensional Visualization of Crystal, Volumetric and Morphology Data. *J. Appl. Crystallogr.* **2011**, *44*, 1272−1276.